

# Channel Modeling for FR3 Upper Mid-band via Generative Adversarial Networks

Yaqi Hu\*, Mingsheng Yin\*, Marco Mezzavilla<sup>†</sup>, Hao Guo\*<sup>‡</sup>, Sundeep Rangan\*

\*NYU Tandon School of Engineering, Brooklyn, NY, USA

<sup>†</sup>Dipartimento di Elettronica, Informazione e Bioingegneria (DEIB), Politecnico di Milano, Milan, Italy

<sup>‡</sup>Department of Electrical Engineering, Chalmers University of Technology, Gothenburg, Sweden

**Abstract**—The upper mid-band (FR3) has been recently attracting interest for new generation of mobile networks, as it provides a promising balance between spectrum availability and coverage, which are inherent limitations of the sub 6GHz and millimeter wave bands, respectively. In order to efficiently design and optimize the network, channel modeling plays a key role since FR3 systems are expected to operate at multiple frequency bands. Data-driven methods, especially generative adversarial networks (GANs), can capture the intricate relationships among data samples, and provide an appropriate tool for FR3 channel modeling. In this work, we present the architecture, link state model, and path generative network of GAN-based FR3 channel modeling. The comparison of our model greatly matches the ray-tracing simulated data.

**Index Terms**—Channel modeling, upper mid-band, 6G, FR3, neural networks, GANs.

## I. INTRODUCTION

With congested sub-6 GHz and the blockage/short-range issues at millimeter wave bands, FR3, also referred to as the upper mid-band (from approximately 7 GHz to 24 GHz) has been attracting research interests from both academic and industrial perspectives [1]. FR3 provides an excellent balance of coverage and bandwidth, while the range of spectrum is large on its own. Nevertheless, with current incumbents such as military radar, radio astronomy, and communication satellites, the radio spectrum resources at FR3 will likely need to be shared.

Spectrum sharing in the upper mid-band has been considered a key challenge in order to fully exploit the FR3 potential, and it will call for channel modeling efforts spanning multiple carrier frequencies. Here, the desired models should be able to capture the joint distribution across multiple bands. There have been recent multi-frequency measurement campaigns [2], [3]. However, these measurements are enormously time-consuming, and adaptive models are still missing.

Data-driven machine-learning methods with minimal assumptions can naturally capture intricate probabilistic relationships. Generative neural networks provide a natural approach to data-driven channel modeling that can broadly represent complex settings, and some early works have successfully trialed generative adversarial networks (GANs) for simple wireless channels [4], [5]. In our previous study [6], we propose a generative model that is constructed from two cascaded

neural networks as shown in Fig. 1: The first network generates the link state (i.e., if the link is in line-of-sight, non-line of sight, or outage) based on the condition vector  $\mathbf{u}$ . The second network generates the path data vector based on the condition vector and link state. Nevertheless, the method proposed in [6] cannot be applied directly to FR3 due to its multi-frequency properties. Moreover, the channel measurements [2], [3] do not provide sufficient data points for training complex neural networks.

In this paper, we propose a GAN-based channel modeling method that aims to capture the characteristics of FR3 multi-band operations. The key differences from [6] are 1) the path generator network uses a GAN, and 2) the data is generated across multiple frequencies. The contributions of the paper are summarized as follows:

- We consider the use of the multi-frequency GAN channel methodology developed in [7]. The benefit of this procedure is that the cross-frequency relations are well captured. The work [7] leveraged the framework for mmWave frequencies. Here, we apply the framework to the upper mid-band and improve the adapt the model in [7] to upper-mid band by a link state predictor.
- We demonstrate that the GAN modeling framework can capture key aspects of the wideband channel. For instance, it can capture the marginal and *joint* distributions of the path loss.
- We demonstrate how the method can be used for assessing inter-frequency tasks. In particular, we evaluate a beamforming approach where the beamforming vector is selected at a lower frequency and then applied at a higher frequency.
- The proposed method is also evaluated by the angles spread of both AoA and AoD for different frequencies.

## II. SYSTEM MODEL

As an extension of our previous study [7] where we presented a general methodology for modeling full double-directional channels at multiple  $M$  frequencies, here, we focus on FR3/upper mid-band [1] and model channel with  $M = 4$  at  $f_1 = 6$  GHz,  $f_2 = 12$  GHz,  $f_3 = 18$  GHz, and  $f_4 = 24$  GHz. In this section, we first present the multi-frequency channel model specifically for FR3. Then, our proposed generative neural network-based modeling method is introduced with a two-stage structure.

The work was supported, in part, by NSF grants 1952180, 2133662, 2236097, 2148293, 1925079, the NTIA, the industrial affiliates of NYU WIRELESS, and by Remcom that provided the Wireless InSite software. Hao Guo was supported by the Swedish Research Council (No. 2023-00272).

### A. Multi-Frequency Channel Model for FR3

In this work, we model a single link, i.e., the channel from a transmitter (TX) to receiver (RX). For instance, the channel between a base station (gNB) and a user equipment (UE) as in cellular applications. With reciprocity, the TX and RX could be reversed. We assume that the channel across the  $M$  frequencies share a common set of  $L$  paths where each path is described by a vector of parameters [7],

$$\chi_\ell = [\tau_\ell, \theta_\ell^{\text{rx}}, \phi_\ell^{\text{rx}}, \theta_\ell^{\text{tx}}, \phi_\ell^{\text{tx}}, G_{\ell 1}, \dots, G_{\ell M}], \quad (1)$$

where  $\tau_\ell$  is the path delay,  $\theta_\ell^{\text{rx}}, \phi_\ell^{\text{rx}}$  are the elevation and azimuth angles of arrival (AoA),  $\theta_\ell^{\text{tx}}, \phi_\ell^{\text{tx}}$  are the elevation and azimuth angles of departure (AoD), and  $G_{\ell 1}, \dots, G_{\ell M}$  are the path gains across the  $M$  frequencies. Here, the implicit assumption is that the path angles and delays are shared across the frequencies. It has been used in the 3GPP statistical model [8] and is physically justified since the waves between the TX and RX at different frequencies generally propagate over the same paths. The multi-frequency channel can then be described by the set of  $L$  paths

$$\mathbf{x} = [\chi_1, \dots, \chi_L]. \quad (2)$$

We will call  $\mathbf{x}$  the *path vector*. This channel description is similar to [6] but with  $M$  path gains per path due to FR3 characteristics. Also, we set  $L = 20$  as it is the default maximum number of paths found by the ray tracer as described below. When there are less than  $L$  paths, say  $L_0 < L$ , we simply set  $G_{\ell m} = 0$  (in linear scale) for all  $\ell > L_0$  and all  $m = 1, \dots, M$ . Moreover, each link also has a condition vector,  $\mathbf{u}$ , which is defined as

$$\mathbf{u} = (d_x, d_y, d_z), \quad (3)$$

i.e., the 3D vector between the TX and RX. Other parameters could be added to  $\mathbf{u}$  such as the antenna heights or cell types.

The statistical channel modeling problem is to model the distribution of the path vector  $\mathbf{x}$  as a function of the link conditions  $\mathbf{u}$ , i.e., the conditional probability distribution  $p(\mathbf{x}|\mathbf{u})$ . In this work, we deploy the so-called generative models and the conditional distribution we are looking for can be represented as a mapping

$$\mathbf{x} = g(\mathbf{u}, \mathbf{z}), \quad (4)$$

where  $\mathbf{z}$  is some random vector with a known distribution. As indicated in [8], generative models provide powerful tools for the evaluations of cellular networks, especially for the multiple-input multiple-output (MIMO) channels. The randomness of the radio channel can be well captured by generative models with path parameters and antenna array assumptions.

### B. Generative Neural Network Modeling

As shown in Fig. 1, our proposed generative neural network model contains two stages: link state predictor network and path generative network.

1) *Link State Model*: The first network – the link state network – takes as an input the condition vector  $\mathbf{u}$  in (3) and generates a random link state, denoted as  $s$ , corresponding to one of three states [9]:

- i) LOS: The LOS path is present, in addition to NLOS paths;
- ii) NLOS: No LOS path, but at least one NLOS path is present;
- iii) Outage: No propagation paths (either LOS or NLOS) exist for this link.

The structure of this network is based on [6]. Specifically, the condition vector  $\mathbf{u}$  is first converted to a 3D distance and elevation distance, denoted as  $\mathbf{u} = (d_{3D}, d_z)$ . Then, the vector  $\mathbf{u}$  is fed to a fully connected neural network with parameters shown in Table I. The output of the network is a 3-way softmax that generates the probabilities of each link state.

2) *Path Generative Network*: The input to the path generative network is the GAN vector  $\mathbf{c} = (\mathbf{u}, s)$  which contains the link condition vector  $\mathbf{u}$  along with the randomly generated link state  $s$ . The goal of the network is to then generate random path vectors  $\mathbf{x}$  in (2) following the conditional distribution  $p(\mathbf{x}|\mathbf{c})$  as observed in the data.

For this purpose, we use a conditional Wasserstein generative adversarial network with gradient penalty (CWGAN-GP) [4], [5] with two components: a *generator*  $\mathbf{G}$  and *critic*  $\mathbf{C}$ . The generator takes the condition vector  $\mathbf{c}$  and some random input  $\mathbf{z} \sim p(\mathbf{z})$  and generates a random path data vector  $\mathbf{x} = \mathbf{G}(\mathbf{c}, \mathbf{z})$  where the vector  $\mathbf{z}$  is called the *latent vector*. As is commonly used in [4], [5], we take its distribution  $p(\mathbf{z})$  to be a unit variance Gaussian vector. Moreover, we set the latent dimension to 20. To ensure the generator matches the data distribution, one can also train a critic function  $\mathbf{C}$  that attempts to discriminate between the generated and true samples. Finally, the generated network is trained with a loss function defined as

$$\underbrace{\mathbb{E}_{\tilde{\mathbf{x}} \sim \mathbb{P}_g} [C(\tilde{\mathbf{x}})] - \mathbb{E}_{\mathbf{x} \sim \mathbb{P}_r} [C(\mathbf{x})]}_{\text{Original critic loss}} + \lambda \underbrace{\mathbb{E}_{\tilde{\mathbf{x}} \sim \mathbb{P}_{\tilde{\mathbf{x}}}} \left[ \left( \|\nabla_{\tilde{\mathbf{x}}} D(\tilde{\mathbf{x}})\|_2 - 1 \right)^2 \right]}_{\text{Gradient penalty}},$$

where  $\mathbb{P}_g$  is the generator distribution implicitly defined by  $\tilde{\mathbf{x}} = \mathbf{G}(\mathbf{c}, \mathbf{z})$ , with  $\mathbf{z} \sim p(\mathbf{z})$ . Also,  $\mathbb{P}_r$  is the distribution of the data points. The loss is optimized via a minimax operation: The critic  $\mathbf{C}$  attempts to minimize the loss to discriminate between the generated and true samples, while the generators attempt to maximize the loss to fake the critic. The minimax is similar to other GANs, but the key concept in the WGAN-GP is that the gradient penalty term avoids mode collapse – see [4], [5] for details. For our application, both the generator and critic are realized with as fully connected neural networks with parameters shown in Table I. Our implementation details are available online at [10].

### III. DATA ACQUISITION: URBAN FR3 CELLULAR SYSTEM WITH RAY TRACING

This methodology is broadly applicable, yet for this study, we focus on evaluating hypothetical systems at four frequencies of 6, 12, 18, and 24 GHz in the upper mid-band band. In

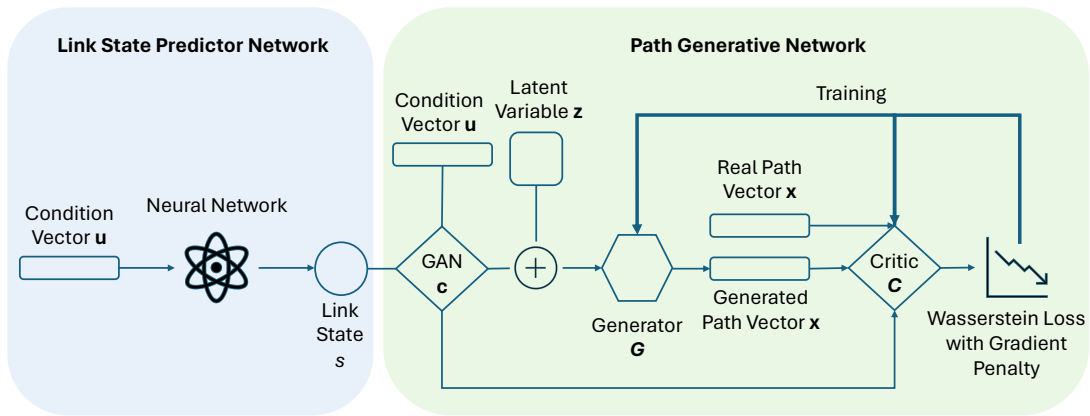


Fig. 1. The architecture for the proposed two-stage generative neural network model.

TABLE I  
GENERATIVE MODEL CONFIGURATION

	Link state prediction	Path GAN critic	Path GAN generator
Num. of inputs	2	180 + 3	20 + 3
Hidden units	[25, 10]	[1120, 560, 280]	[280, 560, 1120]
Num. of outputs	3	1	180
Optimizer	Adam	Adam	Adam
Learning rate	0.001	0.0001	0.0001
Epochs	100	30000	30000
Batch size	200	2048	2048

TABLE II  
MATERIAL PROPERTIES AT DIFFERENT FREQUENCIES: CONDUCTIVITY (S/m) AND PERMITTIVITY (RELATIVE) [15]

Material	6 GHz		12 GHz		18 GHz		24 GHz	
	Con.	Per.	Con.	Per.	Con.	Per.	Con.	Per.
Concrete	.188	5.24	.323	5.24	.443	5.24	.555	5.24
Brick	.032	3.91	.035	3.91	.038	3.91	.040	3.91
Glass	.040	6.31	.100	6.31	.173	6.31	.254	6.31
Plaster	.046	2.73	.088	2.73	.128	2.73	.168	2.73
Wood	.032	1.99	.067	1.99	.104	1.99	.142	1.99
Dry Earth Ground	.649	12.5	2.00	10.0	4.00	7.20	5.60	6.00

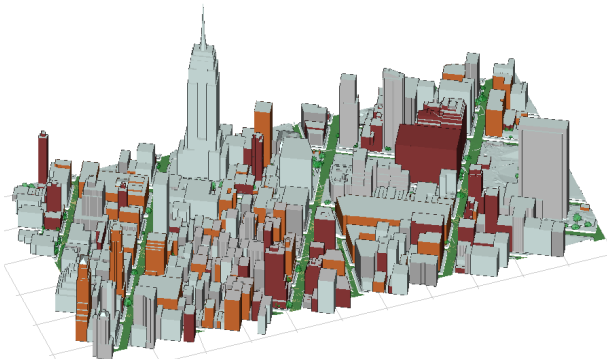


Fig. 2. Ray tracing simulation area representing a  $1100 \times 570 \text{ m}^2$  urban region of NYC.

alignment with recent studies [11], [12], [13], we employ an advanced ray tracing tool, Wireless InSite by Remcom [14], for generating the required datasets for our analysis.

In this work, similar to the configuration in [1], we target a specific area of New York City covering around  $1100 \times 570$  square meters, as shown in Fig. 2. We strategically placed 79 gNBs on building rooftops, achieving a 3-dimensional inter-site distance (ISD) ranging from 100 to 200 meters. This spacing is typical for urban microcellular networks. Additionally, terrestrial UEs were methodically placed 5 meters apart in a grid layout. Importantly, all UEs are positioned 1.6 m above the ground level, and some are located inside buildings to comprehensively simulate the urban cellular landscape. This setup comprises 22,950 UEs, thus establishing  $79 \times 22950 = 1,813,050$  gNB-UE links.

Our ray tracing simulations were conducted independently

at the aforementioned four frequencies. We configured the simulations to consider up to 6 reflections, 1 diffraction, and 1 transmission per path, with no more than 20 paths per link. Moreover, this ray tracing tool captures only paths with a minimum power level of -250 dBm.

The model depicted in Fig. 2 is derived from [16], which provides an accurate depiction of the characteristics of both foliage and building materials. To ensure precise ray tracing across the different frequencies, the properties of materials such as concrete, brick, plaster, wood, glass, and dry earth ground were meticulously detailed, as shown in Table II.

#### IV. MODELING RESULTS

In this section, we present numerical results on the effectiveness of the proposed GAN-based method applied at FR3. As introduced in Section III, the dataset includes 1,813,050 links, each consisting of paths at 6 GHz, 12 GHz, 18 GHz, and 24 GHz, respectively. For our analysis, we randomly selected 30% of the links for training and reserved 10% of the remaining links for testing.

##### A. Path Loss with Omnidirectional Antennas

Our initial assessment focuses on the model's capability to accurately reflect the joint distribution of path loss across two specific frequencies. The evaluation is conducted as follows: Let  $\tilde{\mathbf{x}} = \mathbf{G}(\mathbf{c}, \mathbf{z})$  represent the generated model output, and let  $(\mathbf{c}_i, \mathbf{x}_i)$ ,  $i = 1, \dots, N_{\text{ts}}$  represent the test samples, where each data point consists of the link condition  $\mathbf{c}_i$  and the

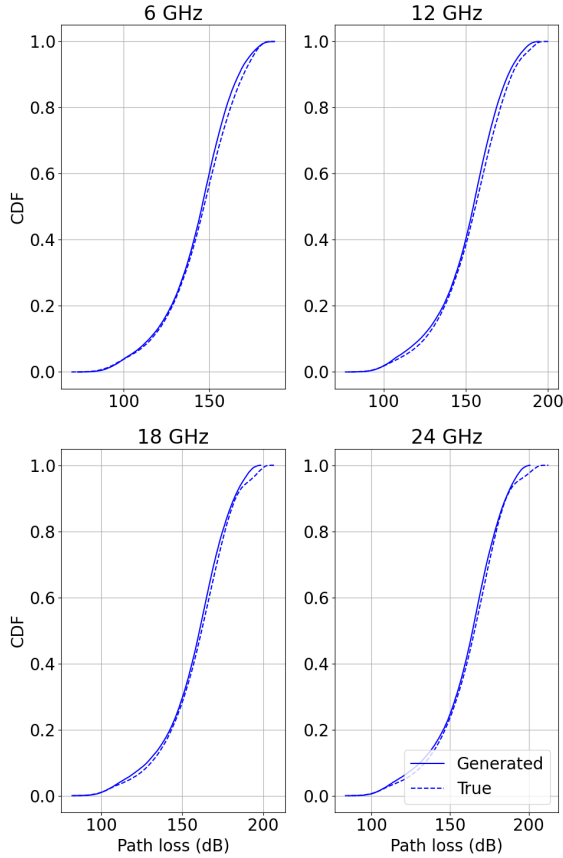


Fig. 3. The CDF of the path loss for links within the test dataset is compared against the CDF of the pass loss for links randomly generated by the trained model.

corresponding path data vector  $\mathbf{x}_i$ . For each test sample, we evaluate the vector

$$\mathbf{v}_i = (v_{i1}, v_{i2}, v_{i3}, v_{i4}) = (\phi_1(\mathbf{x}_1), \phi_2(\mathbf{x}_2), \phi_3(\mathbf{x}_3), \phi_4(\mathbf{x}_4)), \quad (5)$$

where  $v_{ij}$  denotes the omni-directional path loss for sample  $i$  at frequency  $j$  for  $j = 1, 2, 3, 4$ . Here,  $\phi_j(\mathbf{x})$  calculates the omni-directional path loss at frequency  $j$  from the path vector  $\mathbf{x}$ . The omni-directional path loss reflects the path loss that would occur if both the gNB and UE possessed omni-directional antennas.

To assess these values against those generated by the model, for each test sample  $i$ , a random sample  $\mathbf{x}_i^{\text{rnd}} = \mathbf{G}(\mathbf{c}_i, \mathbf{z}_i)$  is generated by the trained generator  $\mathbf{G}$  using a random  $\mathbf{z}_i$  under the same conditions  $\mathbf{c}_i$  as the test data. Then, we compute the set of generated path losses

$$\begin{aligned} \mathbf{v}_i^{\text{rnd}} &= (v_{i1}^{\text{rnd}}, v_{i2}^{\text{rnd}}, v_{i3}^{\text{rnd}}, v_{i4}^{\text{rnd}}) \\ &= (\phi_1(\mathbf{x}_1^{\text{rnd}}), \phi_2(\mathbf{x}_2^{\text{rnd}}), \phi_3(\mathbf{x}_3^{\text{rnd}}), \phi_4(\mathbf{x}_4^{\text{rnd}})). \end{aligned} \quad (6)$$

The distribution of  $\mathbf{v}_i$  and  $\mathbf{v}_i^{\text{rnd}}$  should be closely matched.

Fig. 3 presents the empirical cumulative distribution functions (CDFs) for the marginal distributions of both ray tracing ( $v_{ij}$ ) and model-generated data  $v_{ij}^{\text{rnd}}$  across the four frequencies, i.e., 6, 12, 18, and 24 GHz. As can be seen from the

TABLE III  
MULTI-FREQUENCY SNR SIMULATION PARAMETERS

Parameter	6 GHz	12 GHz	18 GHz	24 GHz
Bandwidth [MHz]	100	200	300	400
gNB URA dims.	$2 \times 2$	$4 \times 4$	$5 \times 5$	$7 \times 7$
UE ULA dims.	$1 \times 2$	$1 \times 2$	$1 \times 3$	$1 \times 3$
Max. TX Power (dBm)	33 (3GPP TR 38.141 [17])			
Sectors for gNBs	3			
UE Noise Figure (dB)	7			
Antenna Pattern	3GPP TR 37.840 [18]			
Down-tilt Angle	$12^\circ$			

plot, the marginal CDFs show great much at all considered frequencies.

Furthermore, a notable observation is that the generator also effectively captures the joint statistics. The first row of Fig. 4 depicts kernel density estimation (KDE) plots of the test data points  $(v_{i1}, v_{i2}, v_{i3}, v_{i4})$  at different frequencies. And the second row shows KDE plots of the generated outputs  $(v_{i1}^{\text{rnd}}, v_{i2}^{\text{rnd}}, v_{i3}^{\text{rnd}}, v_{i4}^{\text{rnd}})$ . From the KDE results, we can observe that the *joint* distributions are also well captured by the proposed scheme.

### B. SNR with Beamforming

To further evaluate the effectiveness of the proposed method, we estimate the AoA and AoD using a reliable lower frequency, specifically 6 GHz, and subsequently apply the derived beamforming vector to higher frequencies: 12 GHz, 18 GHz, and 24 GHz. We summarize the simulation parameters for prospective cellular systems at these frequencies in Table III. The bandwidth allocation for each frequency scales proportionally with the carrier frequency, in line with current deployment strategies. We then calculate the signal-to-noise ratio (SNR) difference between the links generated and those obtained via ray-tracing samples. Figure 5 illustrates that the CDF of the SNR difference between the test and generated data aligns closely across different frequencies.

### C. Root Mean Square (RMS) Angles Spread

The Root Mean Square (RMS) angle spread is critical for evaluating channel models, particularly in the FR3 bands. Figure 6 displays CDF images of the RMS spreads for AoA and AoD. Moreover, to address heterogeneous data types, we align path angles to the LOS direction. Specifically, for preprocessing the AoA, the LOS AoA direction serves as the z-axis in a new spherical coordinate system, facilitating the calculation of azimuth and inclination transformation angles. A similar approach is adopted for the AoD, using the LOS AoD direction. This alignment enables the network to more effectively learn a statistical model relative to the condition vector. According to Figure 6, the model successfully captures the RMS angle spread characteristics at both carrier frequencies, with the spread at 6 GHz being slightly greater than at 18 GHz.

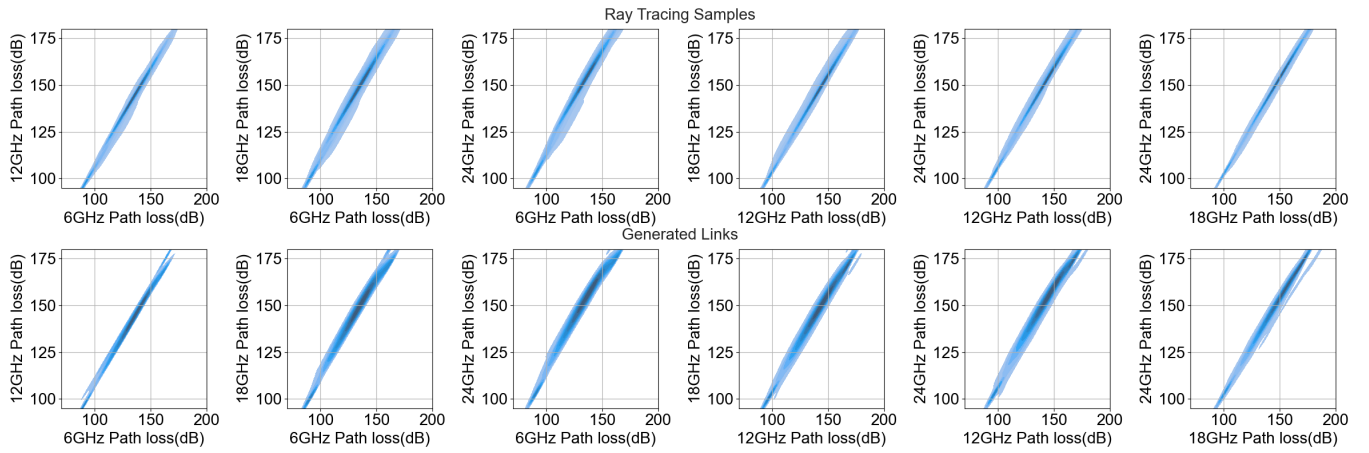


Fig. 4. The KDE plot of bivariate distributions of the path loss at 6 GHz, 12 GHz, 18 GHz, and 24 GHz.

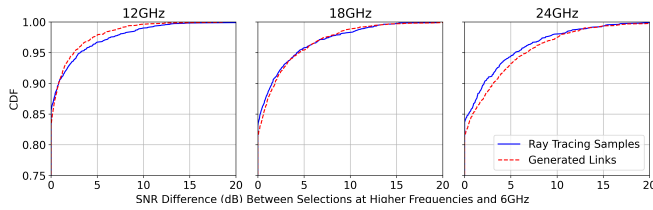


Fig. 5. The CDF plot of SNR differences (in dB) between beam selected by higher frequencies (12 GHz, 18 GHz, and 24 GHz) and beam selected by 6 GHz.

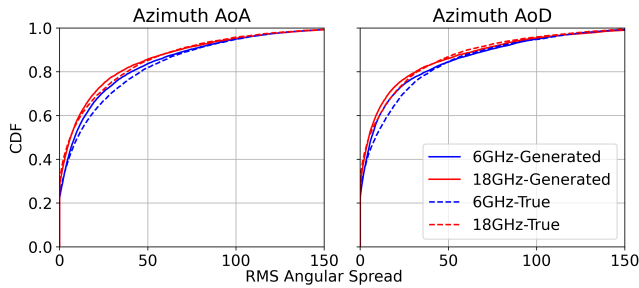


Fig. 6. RMS azimuth AoA/AoD spread, including the zero values

## V. CONCLUSION

This work proposed a GAN-based channel modeling scheme to capture the multi-frequency characteristics at upper mid-band/FR3. With the link state predictor stage, the proposed generative neural network can effectively reflect both marginal and joint channel distributions. The agreements of path loss CDF, KDF, beamforming SNR, as well as RMS distribution together showed great potential for the use of GAN in FR3 channel modeling.

## REFERENCES

- [1] S. Kang, M. Mezzavilla, S. Rangan, A. Madanayake, S. B. Venkatakrishnan, G. Hellboug, M. Ghosh, H. Rahmani, and A. Dhananjay, "Cellular wireless networks in the upper mid-band," *IEEE Open J. Commun. Soc.*, Mar. 2024.
- [2] J. Huang, C.-X. Wang, H. Chang, J. Sun, and X. Gao, "Multi-frequency multi-scenario millimeter wave MIMO channel measurements and modeling for B5G wireless communication systems," *IEEE J. Sel. Areas Commun.*, vol. 38, no. 9, pp. 2010–2025, Sept. 2020.
- [3] Z. Cui, C. Briso-Rodriguez, K. Guan, Z. Zhong, and F. Quitin, "Multi-frequency air-to-ground channel measurements and analysis for UAV communication systems," *IEEE Access*, vol. 8, pp. 110 565–110 574, Jun. 2020.
- [4] I. Gulrajani, F. Ahmed, M. Arjovsky, V. Dumoulin, and A. Courville, "Improved training of Wasserstein GANs," Dec. 2017, [Online]. Available: <https://arxiv.org/abs/1704.00028>.
- [5] M. Arjovsky, S. Chintala, and L. Bottou, "Wasserstein generative adversarial networks," in *Proc. PMLR International conference on machine learning*, Sydney, Australia, 2017, pp. 214–223.
- [6] W. Xia, S. Rangan, M. Mezzavilla, A. Lozano, G. Geraci, V. Semkin, and G. Loiano, "Millimeter wave channel modeling via generative neural networks," in *Proc. IEEE Globecom Workshops*, Taipei, Taiwan, 2020, pp. 1–6.
- [7] Y. Hu, M. Yin, W. Xia, S. Rangan, and M. Mezzavilla, "Multi-frequency channel modeling for millimeter wave and THz wireless communication via generative adversarial networks," in *Proc. IEEE 56th Asilomar Conference on Signals, Systems, and Computers*, Pacific Grove, CA, USA, 2022, pp. 670–676.
- [8] 3GPP Technical Report 38.901, "Study on channel model for frequencies from 0.5 to 100 GHz (Release 16)," Dec. 2019.
- [9] M. R. Akdeniz, Y. Liu, M. K. Samimi, S. Sun, S. Rangan, T. S. Rappaport, and E. Erkip, "Millimeter wave channel modeling and cellular capacity evaluation," *IEEE J. Sel. Areas Commun.*, vol. 32, no. 6, pp. 1164–1179, Jun. 2014.
- [10] S. Rangan, Y. Hu, M. Yin, W. Xia, and M. Mezzavilla, "Multi-frequency millimeter wave channel modeling via generative adversarial network, GitHub repository," Dec. 2021, [Online]. Available: <https://github.com/kmyyayqihu/mmwchanmod-GAN>.
- [11] Y. Hu, M. Yin, S. Rangan, and M. Mezzavilla, "Parametrization and estimation of high-rank line-of-sight MIMO channels with reflected paths," *IEEE Trans. Wireless Commun.*, Apr. 2024.
- [12] M. Yin, A. K. Veldanda, A. Trivedi, J. Zhang, K. Pfeiffer, Y. Hu, S. Garg, E. Erkip, L. Righetti, and S. Rangan, "Millimeter wave wireless assisted robot navigation with link state classification," *IEEE Open J. Commun. Soc.*, vol. 3, pp. 493–507, Mar. 2022.
- [13] W. Khawaja, O. Ozdemir, and I. Guvenc, "UAV air-to-ground channel characterization for mmWave systems," in *Proc. IEEE VTC-Fall*, Toronto, ON, Canada, 2017.
- [14] Remcom, [Online]. Available: <https://www.remcom.com>.
- [15] ITU-R, "Effects of building materials and structures on radiowave propagation above about 100 MHz, Recommendation ITU-R P.2040-2," 2015.
- [16] "GeoPipe: Build the future with interactive 3D models of the real world," [Online]. Available: <https://www.geopipe.ai/>.
- [17] 3GPP Technical Report 38.141, "Base station (BS) conformance testing part 2: Radiated conformance testing," 2017.
- [18] 3GPP Technical Report 37.840, "Study of radio frequency (RF) and electromagnetic compatibility (EMC) requirements for active antenna array system (AAS) base station," 2019.